$CoO-TiO_2$ and WO_3-TiO_2 mixed oxide as photocatalyst for H_2 generation

A. Pérez-Larios, A. Hernández-Gordillo, F. Tzompantzi, R. Gómez
Universidad Autónoma Metropolitana-Iztapalapa, Depto. de Química, Área de Catálisis, Grupo ECOCATAL, Av. San Rafael Atlixco No 189, Del. Iztapalapa, D.F. México, 09340.
e-mail:mciqalex@gmail.com

Abstract

In this work we studied titanium dioxide modified with different percent of mixed oxide either CoO or WO_3 (1.0, 3.0, 5.0 wt.%). The solids were characterized by nitrogen physisorption (BET) and porosity (BJH), XRD patterns and UV-Vis and Raman spectroscopy. The photoactivity was evaluated in an Pyrex reactor of 200 ml using a solution ethanol-water (1:1 molar ratio) and 0.1 g of catalyst using a high pressure Hg lamp (with a wavelength of 254 nm and an intensity of 2.2 mW/cm^2 encapsulated in a quartz tube. The results showed materials with specific surface areas among 89 to 95 m^2/g and 41 to 91 m^2/g respectively with mesopority characteristics. The XRD patterns show the formation of the crystalline anatase phase. The band gap energy (Eg) for the materials were obtained with UV-Vis spectroscopy, the Eg values for both mixed oxide were less to 3.2 eV. In the water splitting reaction samples modified with 5 wt.% of either Co or W present the highest hydrogen production with 1,000 μmol/h and 950 μmol/h respectively.

Key words: Hydrogen production, mixed oxide, sol gel, photocatalysts, UV-vis.

1. INTRODUCTION

An important process for future energy supplies turns to be "photohydrogen" production from water splitting; the photocatalytic processes is clean and employ a renewable source as it has been reported for various systems [1-3]. Titanium dioxide (TiO_2) is considered as the best photocatalysts for dyes degradation [4-9], pesticides [10-14], atmospheric pollutants [15] as well as for the inorganic pollutant removal from wastewater [16,17]. However, the use of TiO_2 as photocatalysts for water splitting is limited by its redox potential referring to the normal hydrogen electrode (NHE). Important studies about hydrogen production have been made to increase the photocatalytic activity of titanium dioxide for the water splitting reaction. In this way, titanium dioxide is modified by doping with Fe, Zn, Cu, Ni, V, Mg, Be and Ni [18,19], or by impregnating with noble metals Pt, Pd, Ir, Rh, Ru [20]. The synthesis of mixed oxides like CuO, ZnO, NiO and CeO with titanium dioxide [21-24], has attracted attention for researchers because they are low cost materials showing important photocatalytic properties. The incorporated oxide effect has been related to oxygen vacancies in its crystal structure [25,26]. In order to improve the titania photocatalysts in the hydrogen production reaction from water splitting, in the present work TiO_2-CoO and TiO_2-WO_3 mixed oxide were prepared by the sol-gel

method. Cobalt oxide and tungsten trioxide has been chosen as co-participant oxide because theirs energetic conduction and valence bands positions are in the favorable redox region for the water splitting [27], additionally it may reduces the recombination rate of photogenerated e^--h^+ pairs [28]. The characterization of the catalysts was realized by nitrogen physisorption, XRD, Raman and UV-Vis spectroscopies. The water splitting reaction was carried out at room temperature using a solution water-ethanol . The ethanol reacts with the photogenerated holes which is an irreversible reaction performed on the semiconductor surface and then the reduction of water to produce hydrogen is improved [29].

2. Experimental

2.1 Catalyst preparation

The nanomaterials TiO_2-CoO and TiO_2-WO_3 with 1.0, 3.0, and 5.0 wt.%, were prepared by the sol-gel method using titanium (IV) butoxide (Aldrich 97%), cobalt nitrate (Reasol 99%) and tungstic acid (Fluka 99%) as precursors: 44 mL of 1-butanol (Aldrich 99.4 %) and 18 mL of distilled water containing the appropriated amount of $Co(NO_3).6H_2O$ were mixed and a few drops of HNO_3 were added in order to obtain pH=3 in the solution. After the solution was heated at 70°C, 44 mL of titanium(IV) butoxide were added drop wise (water/alkoxide molar ratio 8) under magnetic stirring until the gel was formed, maintaining the temperature during 4 h. Afterwards, the solvent was evaporated at 70°C during 24 h and the dried solid was ground to a fine powder in an agate mortar. The obtained xerogel was annealed at 500°C during 5 h in static air atmosphere using a heating rate of 1°C/min; finally the nanomaterials was ground again. As reference pure TiO_2 sample without Co and W was prepared in the same way described above.

2.2 Catalyst characterization

2.2.1 Physisorption analysis

Nitrogen physisorption isotherms were obtained with an automatic Quantachrome Autosorb 3B instrument. Prior to the nitrogen adsorption, all the samples were outgassed overnight at 200° C. The specific surface areas of the samples were calculated from the nitrogen adsorption-desorption isotherms using the BET method, and the mean pore size diameter from the desorption isotherms using the BJH method.

2.2.2 X-ray powder diffraction

The obtained powders TiO_2 and mixed oxide TiO_2-CoO and TiO_2-WO_3 were analyzed by X-ray diffraction using a Bruker D-8 Advance apparatus. The diffraction intensity as a function of the diffraction angle (2θ) was measured between 4 and 70°, using a step of 0.03° and a counting time of 0.3 s per step.

2.2.3 Raman Spectroscopy

Raman spectra were obtained in a spectrometer Renishaw equipment, model MicroRaman Invia, using a object of 100x and was the source monochromatic radiation with a laser Argon, with wavelength of 514.5 nm corresponded a green light and a power out of 25 mW. In the analysis equipment were putting 10 mg of simple in powder of the solids. The analysis range of displacement Raman was of 0 a 1200 cm^{-1}

2.2.4 Infrared FT-IR

The FT-IR studies were realized by IR-Shimadzu equipped with ATR using a wavelength from 500 cm^{-1} to 4000 cm^{-1}.

2.2.5 UV-Vis diffuse reflectance spectroscopy

The UV–Vis diffuse reflectance spectra were obtained with a Varian Cary 100 UV–Vis spectrophotometer coupled with an integration sphere . A sample of MgO with a 100% reflectance was used as a reference.

2.2.6 Photocatalytic H_2 production.

The photoactivity for the hydrogen generation was evaluated using a Pyrex reactor glass of 200 mL containing an aqueous solution water-ethanol (1:1 molar ratio) and 0.1 g of catalysts. The rradiation energy was made using a high pressure Hg lamp (emitting λ=254 nm and intensity of 2.2 mW/cm^2) encapsulated in a quartz tube which was immersed in the solution. The amount of hydrogen produced was followed by gas chromatography using a Varian CP-3800 gas chromatograph equipped with a thermal conductivity detector and with a molecular sieve 5A column (30m length, 0.35mm ID and 50 mm OD).

3. Results and discussion

3.1 N_2 Physisorption

The specific surface areas of the samples annealed at 500° C are summarized in Table 1. The results show that the specific surface area of the TiO_2-CoO and TiO_2-WO_3 semiconductors are higher than that bare TiO_2 obtained . As the amount of Co and W increases the increment of the specific surface area was observed. The areas for the both TiO_2-CoO and TiO_2-WO_3 solids are 90-95 m^2/g and 48-91 m^2/g respectively. This result suggest that the pores of the samples are cylinders perfect and they present an increasing of width pore when the wt.% of W increases.

Table 1. Textural properties, band gap and H_2 production

Catalysts (wt.%)	Area (m^2/g)	Eg (eV)	H_2 Production (μmol/h)	Crystal Size D
Co 1.0	90	1.59	562	12
Co 3.0	93	1.75	864	13
Co 5.0	95	2.44	1,008	14
W 1.0	48	3.02	600	11
W 3.0	53	3.12	884	12
W 5.0	91	3.08	956	13
TiO_2	64	3.2	190	7.2

3.2 X-ray diffraction

The Figure 1 shows the X-ray diffraction patterns for the bare TiO_2 and for the TiO_2 modified with either cobalt oxide and tungsten oxide at 1.0, 3.0 and 5.0 wt.% . The nanocrystalline anatase structure was confirmed by the (1 0 1), (0 0 4), (2 0 0), (1 0 5) and (2 1 1) diffraction peaks [30,33]. The XRD patterns of anatase have a main peak at 2θ = 25.2º corresponding to the 101 plane where as the main peaks of rutile and brookite phases are at 2θ = 27.4º (110 plane) and 2θ = 30.8º (121 plane), respectively. Therefore, both rutile and brookite phases were not detected [31,32]. The XRD patterns didn't show any Co and W phase (even for 5% TiO_2-CoO and TiO_2-WO_3 samples) indicating that Co and W ions are uniformly dispersed into the anatase crystallites [34,35]. The reflections of the pure TiO_2 crystal (is quite similar to that of CoO-TiO_2 and WO_3-TiO_2 (samples b to g, in figure 1) at different content of either Co and W. In another hand the average particle size was estimated using the Scherrer equation from the anatase (2θ =25.2, 37.8, and 48.1º) diffraction peaks : $D = K\lambda / (\beta \cos \theta)$. where D is the crystal size of the catalyst, λ *is* the X-ray wavelength (1.54056 Å), β *is* the full width at half maximum of the diffraction peak (radian), $K\alpha$ is a coefficient (0.89) and θ is the diffraction angle at the maximum peak. Average crystal sizes calculated of both TiO_2-CoO and TiO_2-WO_3 are around 12-14 nm and 11-13 nm, respectively.

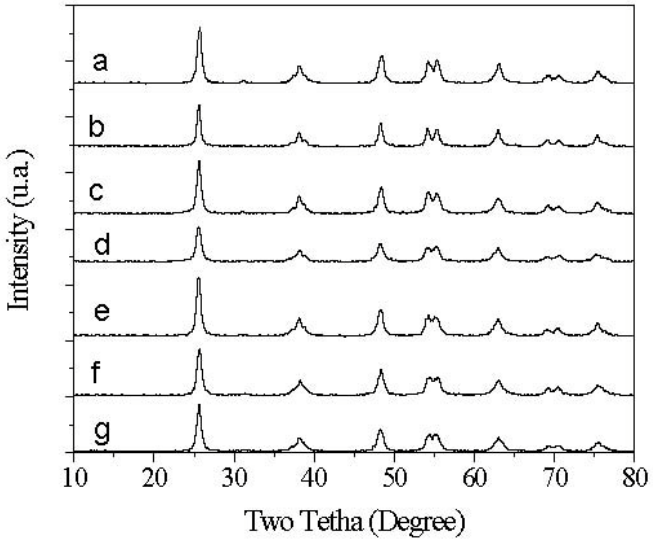

Figure 1. XRD of mixed oxide, TiO_2-CoO and TiO_2-WO_3.
(a:TiO_2, b:CoO 1.0wt.%, c: CoO 3.0wt.%, d: CoO 5.0wt.% , e: WO_3 1.0wt.%, f: WO_3 3.0wt.%, g: WO_3 5.0wt.%)

3.3 Raman Spectroscopy

Raman spectra of all samples are shown in Fig. 2. We can observe four Raman peaks to 145.8 cm^{-1}, 397.9 cm^{-1}, 513 cm^{-1} y 640.7 cm^{-1}; which are characteristic of anatase phase assigned to the modes 2B1g and 2Eg, respectively [36,38]. Moreover, the intensity of the Raman peaks decrease as the metal content increase. This behavior suggests that the metal is into the structure as was confirmed by X-ray.

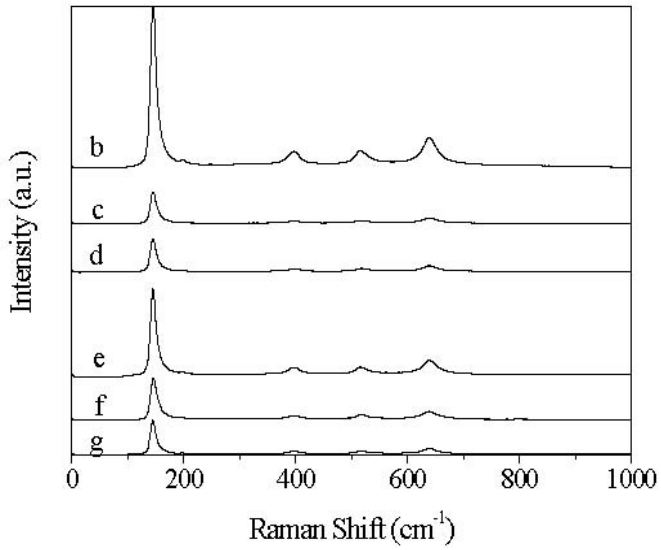

Figure 2. Spectrum Raman of mixed oxide, TiO_2-CoO and TiO_2-WO_3.

(b: CoO 1.0 wt.%, c: CoO 3.0 wt.%, d: CoO 5.0 wt.% , e: WO_3 1.0 wt.%, f: WO_3 3.0 wt.%, g: WO_3 5.0 wt.%)

3.4 FT-IR Spectroscopy

FT-IR spectra of TiO_2 and 1.0, 3.0 and 5.0 wt.% Co and W samples (Fig. 3) show peaks corresponding to stretching vibrations of the O-H and bending vibrations of the adsorbed water molecules. The intensity of these peaks in 3350-3450 cm^{-1} is low because the water was eliminated by annealing of the samples (not shown in the figure) [39]. The broad intense band below 1200 cm^{-1} associated to the Ti-O-Ti vibrations shift to lower wavenumbers and turn sharpening from "b" to "g" This behavior can be explained by the decreasin in nanoparticles size of the catalyst with increasing of the content of either Co and W. In addition, the hydroxyl groups on TiO_2 surface increase with the increasing of the content of Co and W ,. The band at 1389 cm^{-1} associated to the bending vibrations of the C-H bond in the mixed oxide catalysts was not observed [39].

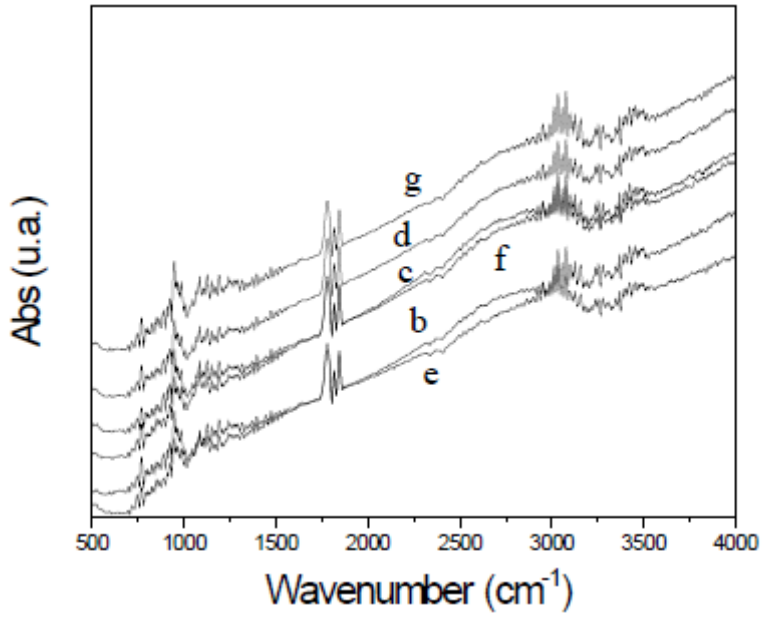

Figure 3. FT-IR spectrum of TiO_2, TiO_2-CoO and TiO_2-WO_3.
(b: CoO 1.0 wt.%, c: CoO 3.0 wt.%, d: CoO 5.0 wt.% , e: WO_3 1.0 wt.%, f: WO_3 3.0 wt.%, g: WO_3 5.0 wt.%)

3.5 UV-Vis Diffuse Reflectance Spectroscopy (DRS)

The electronic properties of the different titania samples were studied whose corresponding spectra are provided in Fig. 4. The absorption spectrum of TiO_2 consists of a single intense broad absorption around 400 nm associated to the charge-transfer from the valence band (mainly formed by 2p orbitals of the oxide anions) to the conduction band (mainly formed by 3d t2g orbitals of the Ti^{4+} cations) [40]. This absorption band is similar to the obtained from TiO_2-WO_3 mixed oxide. The TiO_2 and TiO_2-WO_3 mixed oxide showed absorbance in the shorter wavelength

region whereas TiO_2-CoO samples showed a red shift in the absorption onset value. The transitional metal ions into TiO_2 could shift theirs optical absorption edge from UV to visible light range, but no prominent change in the TiO_2 band gap was observed [34].

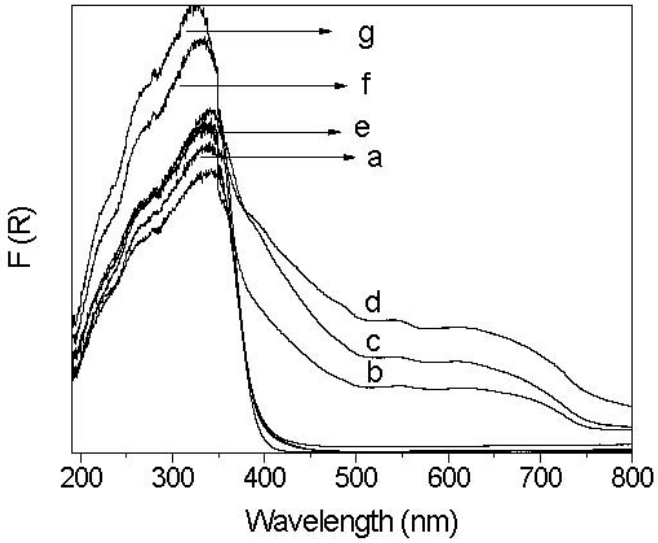

Figure 4. DRS spectrum of TiO_2, TiO_2-CoO and TiO_2-WO_3.
(a: TiO_2, b: CoO 1.0wt.%, c: CoO 3.0wt.%, d: CoO 5.0wt.% , e: WO_3 1.0wt.%, f: WO_3 3.0wt.%, g: WO_3 5.0wt.%)

3.5 Test Production

The Fig. 5 shows the profile of the hydrogen production as a function of the irradiation time for bare TiO_2, TiO_2-CoO and TiO_2-WO_3. We can see that the hydrogen generation increases with the increasing of the content of either Co or W . The hydrogen production from bare TiO_2 is 190 μmol/h. An important effect of cobalt oxide is observed, the H_2 generation using either TiO_2-CoO or TiO_2-WO_3 at 5 wt% is 1000 and 900 μmol/h, respectively, and those values represent an increasing of 500 percent approximately. In this case of the samples with 5 wt. % of either CoO or WO_3 the hydrogen photocatalytic production was improved. Those results are enhancement in comparison with titania nanotubes impreganted with Ir and Co [41] nanocomposites of CoO [42], Pt loaded TiO_2 [43] WO_3-TiO_2 [44].

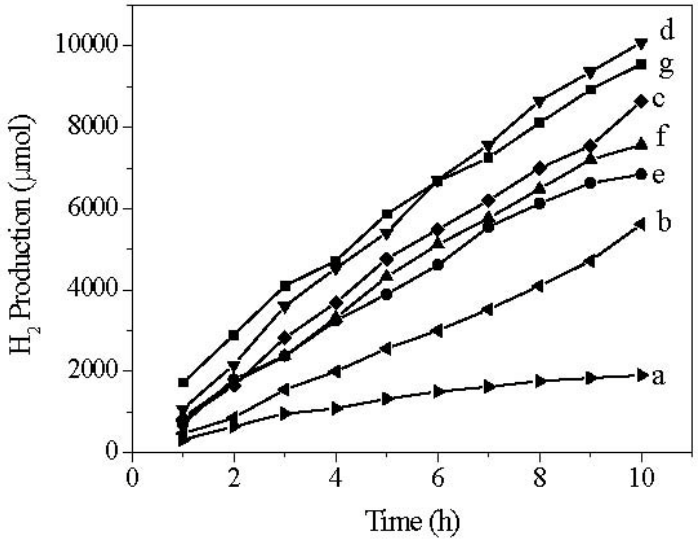

Figure 5. Profile of H_2 production with TiO_2, TiO_2-CoO and TiO_2-WO_3.
(a: TiO_2, b: CoO 1.0wt.%, c: CoO 3.0wt.%, d: CoO 5.0wt.% , e: WO_3 1.0wt.%, f: WO_3 3.0wt.%, g: WO_3 5.0wt.%)

4. Conclusion

TiO_2, TiO_2-CoO and TiO_2-WO_3 nanoparticles were obtained by the solgel method. Among all of the samples only anatase phase was confirmed from the XRD results. The results obtained from the XRD, UV-Vis indicate that the incorporation of either Co or W in TiO_2 was realized, causing that the grain size decreases. Moreover, the absorption bands shifts to lower wavelengths (red shift) and the surface area decrease due to the agglomeration of the particles. The photocatalytic activity of hydrogen production under UV irradiation reveal high activity in presence of the mixed oxide. The TiO_2 modified with CoO at 5.0 wt.% is the best catalyst that exhibit the highest photocatalytic activity in the hydrogen production reaction.

References

[1] N. Arai, N. Saito, H. Nishiyama, K. Domen, H. Kobayashi, K. Sato, Y. Inoue, Catal. Today., 129, 407, (2007).
[2] S. Shen, L. Zhao, L. Guo, Int. J. Hydrogen Energy 35, 10148, (2010).
[3] X. Zhang, D. Jing, L. Guo, Int. J. Hydrogen Energy 35, 7051 (2010).
[4] J. Zitaa, J. Krýsa, U. Černigoj, U. Lavrenčič-Štangar, J. Jirkovsky, J. Rathouský, Catal. Today 161, 29-34 (2011).
[5] M. L. Satuf, M. J. Pierrestegui, L. Rossini, R. J. Brandi, O. M. Alfano, Catal. Today 161, 121-126 (2011).
[6] Y-H Tseng, C-H Kuo., Catal. Today (2011), doi:10.1016/ j.cattod.2011.02.011.
[7] M. Uzunova-Bujnova, R. Kralchevska, M. Milanova, R. Todorovska, D. Hristova, D. Todorovsky, Catal. Today 151, 14-20 (2010).
[8] S. Mozia, Catal. Today 156, 198-207 (2010).
[9] C.A. Castro-López, A. Centeno, S.A. Giraldo, Catal. Today 157, 119-124 (2010).
[10] V. Rodríguez-González, M.A. Ruiz-Gómez, L.M. Torres-Martínez, R. Zanella, R. Gómez, Catal. Today 148, 109-114 (2009).
[11] A. M.T. Silva, C. G. Silva, G. Drazic, J. L. Faria, Catal. Today 144, 13-18 (2009).
[12] A. Kubacka, G. Colón, M. Fernández-García, Catal. Today 143, 286-292 (2009).
[13] C. Guzmán, G. del Ángel, R. Gómez, F. Galindo-Hernández, C. Ángeles-Chavez. Catal. Today, 166, 146-151 (2010).
[14] R. López, R. Gómez, M. E. Llanos, Catal. Today 148, 103-108 (2009).
[15] C. L. Bianchi, G. Cappelletti, S. Ardizzone, S. Gialanella, A. Naldoni, C. Oliva, C. Pirola, Catal. Today 144, 31-36 (2009).
[16] A. Bernabeu, R.F. Vercher, L. Santos-Juanes, P.J. Simón, C. Lardín, M.A. Martínez, J.A. Vicente, R. González, C. Llosá, A. Arques, A.M. Amat, Catal. Today 161, 235–240 (2011).
[17] P-S Yapa, T-T Lima, M. Srinivasan, Catal. Today 161, 46–52 (2011).
[18] IH Tseng, CSW Jeffrey, Catal. Today, 97, 113–9 (2004).
[19] S. Sreethawong, Y. Suzuki, S. Yoshikawa, Int. J. Hydrogen Energy 30, 1053–62 (2005).
[20] A. Erdóelyi, J. Raskó, T. Kecskés, M. Tóth, M. Dömök, K. Baán, Catal. Today 116, 367–376 (2006).
[21] L.S. Yoong, F.K. Chong, B. K. Dutta, Energy 34, 1652–1661 (2009).
[22] D. V. César, R. F. Robertson, N. S. Resende, Catal. Today 133–135, 136–141 (2008).
[23] T. Sreethawong, Y. Suzuki, S. Yoshikawa, Int. J. Hydrogen Energy 30, 1053 – 1062 (2005).
[24] F. Galindo-Hernández, R. Gómez, J. Photochem. Photobiol. A: Chem. 217, 383–388 (2011).
[25] I. Nakamura, N. Negishi, S. Kutsuna, T. Ihara, S. Sugihara, K. Takeuch, J. Mol. Catal. A: Chem. 161, 205–212 (2000).
[26] T. Ihara, M. Miyoshi, Y. Iriyama, O. Matsumoto, S. Sugihara, Appl. Catal. B: Environ. 42, 403–409 (2003).
[27] S. Rehman, R. Ullah, A.M. Butt, N.D. Gohar, J. Hazard. Mat., 170, 560–569 (2009).
[28] R.M. Navarro, F. del Valle, J.A. Villoria de la Mano, M.C. Alvarez-Galvan, J.L.G. Fierro. Adv. Chem. Engin., 36, 111-141 (2009).
[29] J. Bandara, CPK Udawatta, CSK Rajapakse, Photochem. Photobiol. Sci, 4, 857–61 (2005).

[30] H. Ogawa, A. Abe, J. Electrochem. Soc. 128, 685 (1981).
[31] K.V. Baiju, P. Shajesh, W. Wunderlich, P. Mukundan, S.R. Kumar, K.G.K. Warrier, J. Mol. Catal. A 276, 41 (2007).
[32] K.M.K. Srivatsa, M. Bera, A. Basu, Thin Solid Films 516, 7443 (2008).
[33] V. Chakrapani, J. Thangala, M. Sunkara. Int. J. Hydrogen Energy 34, 9050-9059 (2009).
[34] J.C.S. Wu, C.H. Chen, J. Photochem. Photobiol. A, 163, 509 (2004).
[35] L. Chen, J. Li, M. Ge, R.Zhu. Catal. today 153 (2010).
[36] W. F. Zhang, Y. L. He, M. S. Zhang, Z. Yin, Q. Chen, J. Phys. D: Appl. Phys., 33, 912 (2000).
[37] K. Ishikawa, K. Yoshikawa, N. Okada, Phys. Rev. B, 37, 5852 (1988).
[38] T. Ohsaka, F. Izumi, Y. Fujiki, J. Raman Spectroscopy, 7, 321 (1978).
[39] W. Hung, S. Fu, J. Tseng, H. Chu, T. Ko, Chemosphere, 66, 2142 (2007).
[40] N. Venkatachalam, M. Palanichamy, V. Murugesan, J. Mol. Catal. A, 273, 177 (2007).
[41] M. A. Khan, O.B. Yang. Catalysis Today, 146, 177-182 (2009).
[42] J. Yan, H. Yang, Y. Tang, Z. Lu, S. Zheng, M. Yao, Y. Han. Renewable Energy, 34 2399-2403 (2009).
[43] Tao Chen, Zhaochi Feng, Guopeng Wu, Jianying Shi, Guijun Ma, Pinliang Ying, and Can Li. J. Phys. Chem. C, 111, 8005-8014 (2007).